

# ON TWO DISTINCT SHOCKS DURING THE FLARE OF 9 JULY 1996

A. KLASSEN<sup>1</sup>, M. KARLICKÝ<sup>2</sup>, H. AURASS<sup>1</sup> and K. JIŘIČKA<sup>2</sup>

<sup>1</sup>*Astrophysikalisches Institut Potsdam, An der Sternwarte 16, D-14482 Potsdam, Germany*

<sup>2</sup>*Astronomical Institute of the Academy of Sciences of Czech Republic, 251 65 Ondřejov, Czech Republic*

(Received 8 October 1998; accepted 12 May 1999)

**Abstract.** Due to the emission of shock-accelerated electrons, broadband radio observations display propagating super Alfvénic shock waves in the low corona ('type II bursts'). We study the 9 July 1996 flare (AR NOAA 7978) focusing on the aspect of shock generation. This event's radio spectrogram shows two different type II bursts in sequence. Radio imaging data (Paris, Meudon Observatory) reveal that both bursts appear at different sites above the H $\alpha$  flare. The driver of the first type II burst seems to propagate with twice the speed of the second one. The projected source site of the first type II burst (seen earlier and at higher frequencies) is spatially situated further away from the H $\alpha$  flare site than the source of the second type II burst. We try to understand this by comparing with *Yohkoh* soft X-ray images. The first shock source occurs near the top of high soft X-ray loop structures. Its driver can be a guided fast mode magnetic disturbance. The second type II source appears in-between two high soft X-ray loop systems. This might be a piston-driven disturbance powered by an evaporation front. We get a consistent picture only by assuming a very inhomogeneous Alfvén speed in the active region's atmosphere.

## 1. Introduction

Solar type II bursts are generally ascribed to large-scale coronal shock waves. The origin of these disturbances has still not doubtless been identified. Different aspects of type II burst observations are summarized in Nelson and Melrose (1985), Mann (1995), and Aurass (1997, with references to earlier work). Recent theoretical work on electron acceleration in coronal shocks was published by Mann, Classen, and Aurass (1995), Mann and Classen (1995), and Classen and Mann (1997). In a recent attempt to trace the type II radio signature back to lower atmospheric layers, Vršnak *et al.* (1995, with references to earlier work) found that the peak time of the microwave burst is a plausible estimate of the ignition time of the disturbance. This study has been extended based on digitally recorded radio spectra, high time resolution radio imaging data, and soft X-ray *Yohkoh* images by Klassen *et al.* (1999). These authors discovered two radio spectral patterns which systematically precede the type II burst lanes (the type II precursor and the arc pattern). This shows that the driving disturbance exists before the type II radio burst. The very first high-frequency type II burst signature\* is always excited at the top of soft X-ray loop

\*We use the term 'high frequency' for fundamental mode emission with a start frequency greater than 100 MHz.



structures which touch the  $H\alpha$  flare site at least with one footpoint. This confirms earlier results obtained with the Culgoora radioheliograph (cf., Stewart, 1977). The alignment of sources at successively lower frequencies is often non-radial. It tends to move away from the active region (cf., Nelson and Robinson 1975; Klassen *et al.*, 1999).

The relation between flares, coronal mass ejections (CMEs) and coronal (metric) type II bursts is still a matter of debate. Simultaneous radio and optical observations seem to tell that type II bursts are produced by the flare blast wave (cf., Wagner and MacQueen, 1983). The same authors point out that the type II burst sites may well be determined by transient coronal density structures. Gopalswamy and Kundu (1992) collected all CME events with simultaneous radio imaging and found that most type II sources appeared well behind the CME's leading edge. Other results (Sheeley *et al.*, 1984; Robinson and Stewart, 1985) underline a close association between type II and CME events.

In the present paper we focus on an event with at least two type II bursts in sequence and ask for the corresponding drivers or wave modes, respectively. Let us summarize possible coronal shock wave exciters during a flare event.

- We argue that at the very onset of magnetic field reconnection (e.g., Priest, 1996) a fast-mode MHD disturbance escapes as the fastest travelling signal. This is predicted by numerical simulations (e.g., Ugai, 1982; Karlický, 1988).

- Thereafter, a thermal wave front, also named thermal conduction front, ion-acoustic turbulent front (see, e.g., Tandberg-Hanssen and Emslie, 1988) is expected propagating with the sound speed (or supersonic).

- A steady reconnection site should be surrounded by two standing slow-mode shock waves and\* also by stationary fast-mode shocks. There, expelled hot matter (reconnection jets) is transformed from a super Alfvénic to a sub Alfvénic state (e.g., Forbes and Priest, 1983; Tsuneta and Naito, 1998). Until now, corresponding radio shock signatures have not yet been identified.

- In closed magnetic loops, strong fluxes of accelerated particles hit dense chromospheric layers. Pairwise hard X-ray sources (Kosugi, 1993) are considered as evidence for this bombardment. The chromospheric plasma is heated and, due to the corresponding pressure increase, an evaporation shock is generated in front of the rising hot matter (Somov, 1992).

- By timing arguments the head-on boundary of a CME is a less relevant candidate for driving coronal type II bursts quite in contrast with interplanetary (very low frequency) type II bursts (e.g., Aurass, 1997). This view is supported by recent (still rare) comparisons of radio imaging data with SOHO EIT and LASCO data (Klein *et al.*, 1997) as well as by statistical work about low-frequency radio observations in space (Gopalswamy *et al.*, 1998).

In the following, we try to identify the driving agents of coronal shock waves during the 9 July 1996 flare event.

\*Under a specific geometry.

TABLE I  
Summary of radio, X-ray, and H $\alpha$  observations

| Time UT           | Radio observations,<br>structure and range | HXR<br>(keV)   | H $\alpha$ and SXR        |
|-------------------|--|----------------|---------------------------|
| Preheating phase  |  |                |                           |
| 09:02–09:04       |  |                | start, H $\alpha$ and SXR |
| 09:07:58          |  | start, 25–50   |                           |
| 09:08:07(20)      | start, 8 GHz                               |                |                           |
| 09:08:30          | start, 3 GHz                               |                |                           |
| Impulsive phase   |  |                |                           |
| 09:08:35          |  | start, 25–50   |                           |
| 09:08:54          | start, FDB, 2.1–1.4 GHz                    |                | H $\alpha$ kernel         |
| 09:09:00          | start, drift-continuum                     | start, 100–300 |                           |
| 09:09:40          |  | max, 25–1000   |                           |
| 09:09:43          | maximum at 8 GHz                           |                |                           |
| 09:10:10          | maximum at 3 GHz                           |                |                           |
| 09:10:40          | maximum at 1 GHz                           |                |                           |
| 09:10:50          | maximum at 0.8 GHz                         |                |                           |
| Decay phase       |  |                |                           |
| 09:10:30–09:11:30 | first type II, 750–450 MHz                 |                |                           |
| 09:11:07–09:13:10 | second type II, 320–160 MHz                |                | max, H $\alpha$ and SXR   |
| 09:13–10:30       | broadband cm- dm-activity                  |                |                           |
| 09:16             |  | end            |                           |

FDB – fast-drift bursts; only the ranges of type II harmonic lanes are given.

## 2. Observations

The well-known two-ribbon 1B/X2.6 flare on 9 July 1996 (Aurass *et al.*, 1997; Mann *et al.*, 1997; Pick *et al.*, 1997; Dryer *et al.*, 1998; Hudson *et al.*, 1998) was the first major flare after the recent minimum of solar activity. It occurred in association with a huge coronal mass ejection (CME) at S10 W30 in active region AR 7978. An intense radio type II and IV burst emission was observed. Kosovichev and Zharkova (1998) discovered helioseismic disturbances due to this flare. Table I gives a synopsis of some stages of the flare evolution.

For our analysis we used the following data sources: the spectrographic observations were carried out with the spectrographs of Potsdam–Tremisdorf (40–800 MHz) and Ondřejov (1000–4300 MHz) Observatories (Mann *et al.*, 1992; Jiříčka *et al.*, 1993). The radio heliographic data (courtesy K.-L. Klein) were ob-

tained by the Nancay radioheliograph (NRH, The Radioheliograph Group, 1993). For use in the present paper, the NRH data have been integrated over 0.7 s. We only show in this paper the radio source centroid positions.

Further, we used BATSE hard X-ray (HXR) observations in the energy range 25–100 keV with a time resolution of 1.024 s, GOES soft X-ray (SXR) flux data, and *Yohkoh* soft X-ray telescope (SXT) pre- and post-flare full-frame images (Tsuneta *et al.*, 1991). These data were kindly provided by NASA/GSFC SDAC and Mullard SSL, respectively. The H $\alpha$  images were kindly supplied by San Vito Observatory, a magnetogram from SOHO/MDI (Scherrer *et al.*, 1995) was used, too.

## 2.1. ACTIVE REGION STRUCTURE AND EVOLUTION

The activity evolution in AR 7978 was summarized by Hudson *et al.* (1998) and Dryer *et al.* (1998). On 8 July, a rapid sunspot area increase is reported changing the magnetic configuration. In the penumbra of the middle spot of the group new magnetic flux appeared forming a  $\delta$ -configuration. According to radio spectral data, about 1 hour before the flare (07:30–07:55 UT) a huge CME is formed. There are no EIT data of the flare due to technical problems with SOHO. LASCO images of the CME are available for the afternoon hours only (Dryer *et al.*, 1998; Aurass *et al.*, 1997).

The H $\alpha$  flare emission started at 09:05:29 UT. First, a weak brightening and flare knot formation is reported. In the following we consider the H $\alpha$  knots to be the source sites of the HXR emission. The knots appear on both magnetic polarities above the  $\delta$ -configuration of the middle spot. A more essential H $\alpha$  brightening started at the same position at 09:08:59 UT. Later, several bright knots appeared forming both H $\alpha$  ribbons step by step. The ribbons are S-shaped and form an E–W extended pair between the two main sunspots (see Figure 1 at 09:10:29 UT). The length of the flare ribbons was about 69 000 km. During the decay phase the ribbons are connected by post-flare H $\alpha$  loops in emission.

## 2.2. THE SXR MORPHOLOGY

Some representative *Yohkoh*-SXT images before and after the flare are shown in Figure 2. Before the flare (09:02 UT) bright bubble-like structures outline closed magnetic fields corresponding to three bright SXR loop systems. One system (L1) is inclined in the west-northwest direction. The second loop system (L2) is inclined in the southwest direction. The third system consists of low lying loops (L) situated between L1 and L2 (compare the scheme in Figure 4). The L system seems to be connected with the leading and the middle spots in AR 7978. There is also a faint loop (L3) visible connecting the top of L1 and one leg of the L2 system, in projection. After the flare (10:24 UT) the L3 loop is missing. Another faint looplike connection L4 seems to now connect the tops of L1 and L2.

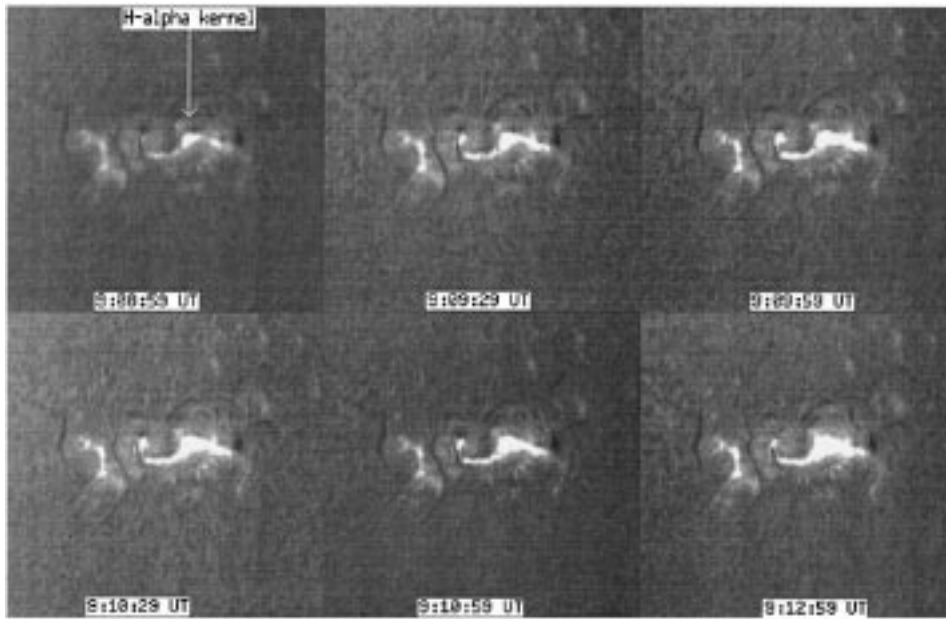


Figure 1. A sequence of  $H\alpha$  images during the flare of 9 July 1996 in AR 7978. The emission is characterized by E–W aligned and S-shaped flare ribbons between two sunspots. The activity starts at 09:05:29 UT with a weak brightening and the formation of a flare knot ( $H\alpha$  kernel) of both polarities above the middle spot, which had a  $\delta$ -configuration. A more essential brightening starts at the same position at 09:08:59 UT. Then, step by step, both  $H\alpha$  ribbons appear (09:09:59 UT). During the decay phase the two ribbons near the  $H\alpha$  kernel change character: they are connected by low  $H\alpha$  loops in emission.

### 2.3. RADIO OBSERVATIONS

A composite dynamic spectrum in the range 40–4300 MHz is shown in Figure 3 together with HXR and SXR data. The flare started at about 09:04 UT with a slow rise (preheating stage). The impulsive phase followed at 09:08:54 UT first in the 1400–2100 MHz frequency range with a group of fast-drift bursts (FDB, henceforth). Further, a slowly negatively drifting continuum appeared between 1000–4300 MHz. After 09:10:30 UT, a group of two type II bursts occurred followed by repeated maxima of broadband continuum emission. It is difficult to recognize the double role of the type II burst in the spectral data alone. There are no meter wave type III bursts preceding the type II emission (see also Mann *et al.*, 1997).

The FDB at 09:08:54 UT coincide with the onset of the HXR emission in the range 100–300 keV. With the given time resolution of radio spectra (0.1 s) the drift rate of individual bursts is infinite. The bursts have well defined cut-offs at high and low frequencies. At 09:09:32 UT the outer envelope of the FDB burst patch starts gradually drifting toward lower frequencies. The leading edge of the continuum drifts towards lower frequencies with a mean rate of  $D_f = 25\text{--}30 \text{ MHz s}^{-1}$

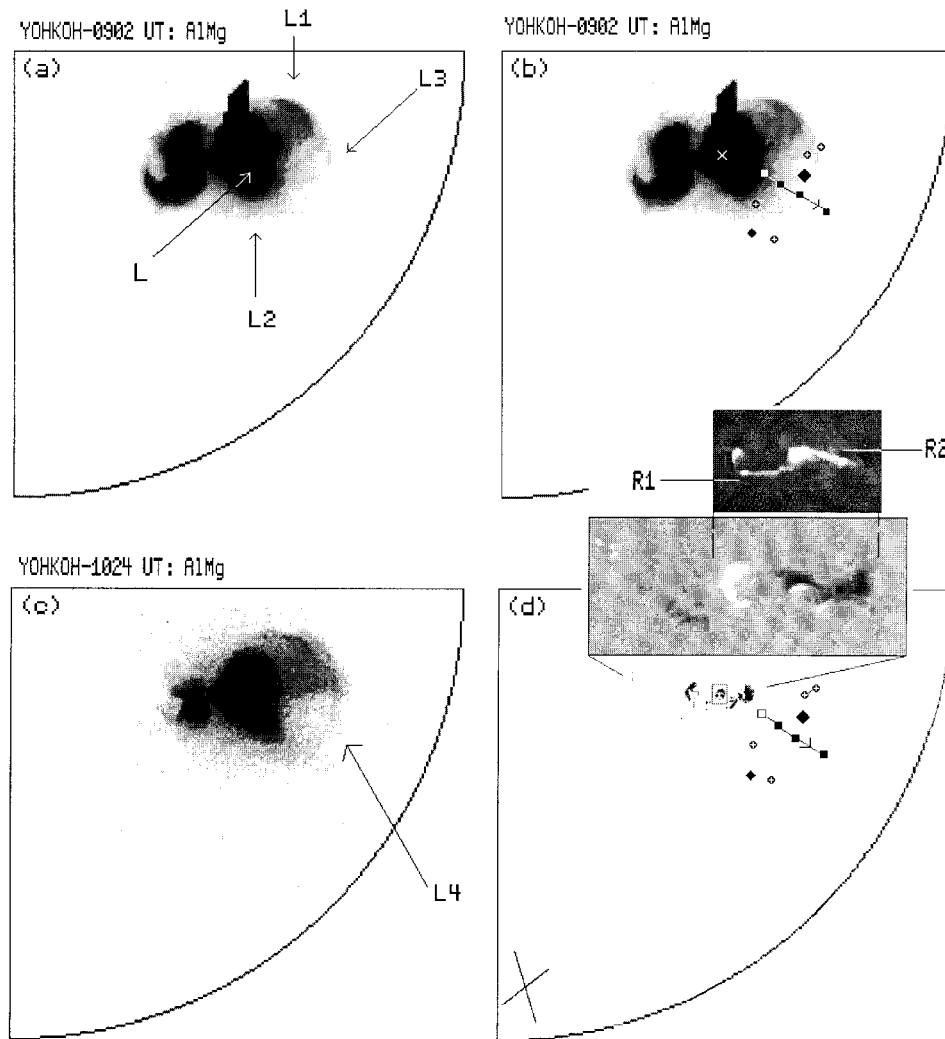


Figure 2. A superposition of the radio source centroid (NRH), soft X-ray (*Yohkoh*),  $H\alpha$  and magnetographic (MDI, SOHO) images observed on 9 July 1996. (a) *Yohkoh*-SXT image at 09:02 UT. Arrows point at loop systems L, L1, L2, L3, and L4. (b) The radio source centroids overlaid onto the *Yohkoh*-SXT image (09:02 UT, AIMg-filter, exposure 0.668 s). Radio centroid positions: first type II burst: big black  $\diamond$  – harmonic mode source, small black  $\diamond$  – fundamental mode source. The second type II burst in the harmonic mode:  $\square$  and  $\blacksquare$ . The arrow points to the trace of the second type II source. Black  $\diamond$  with white cross – broadband continuum source after disappearance of the type II bursts.  $\times$  –  $H\alpha$  flare position. (c) *Yohkoh*-SXT image at 10:24 UT. The loop system L4 is shown by the arrow. The difference of the structure before the flare (a) is visible: the L3 loop is missing, the new L4 system is formed. (d) A superposition of the radio source centroids onto the sunspots drawings (Mt. Wilson Observatory). Inset: *bottom* – magnetographic images (09:40 UT, MDI, SOHO) and *top* – enlarged  $H\alpha$  (09:09:29 UT) images, R1 and R2 – the flare ribbons (compare Figure 1). Big cross – the average halfwidth of type II sources at 327 MHz.

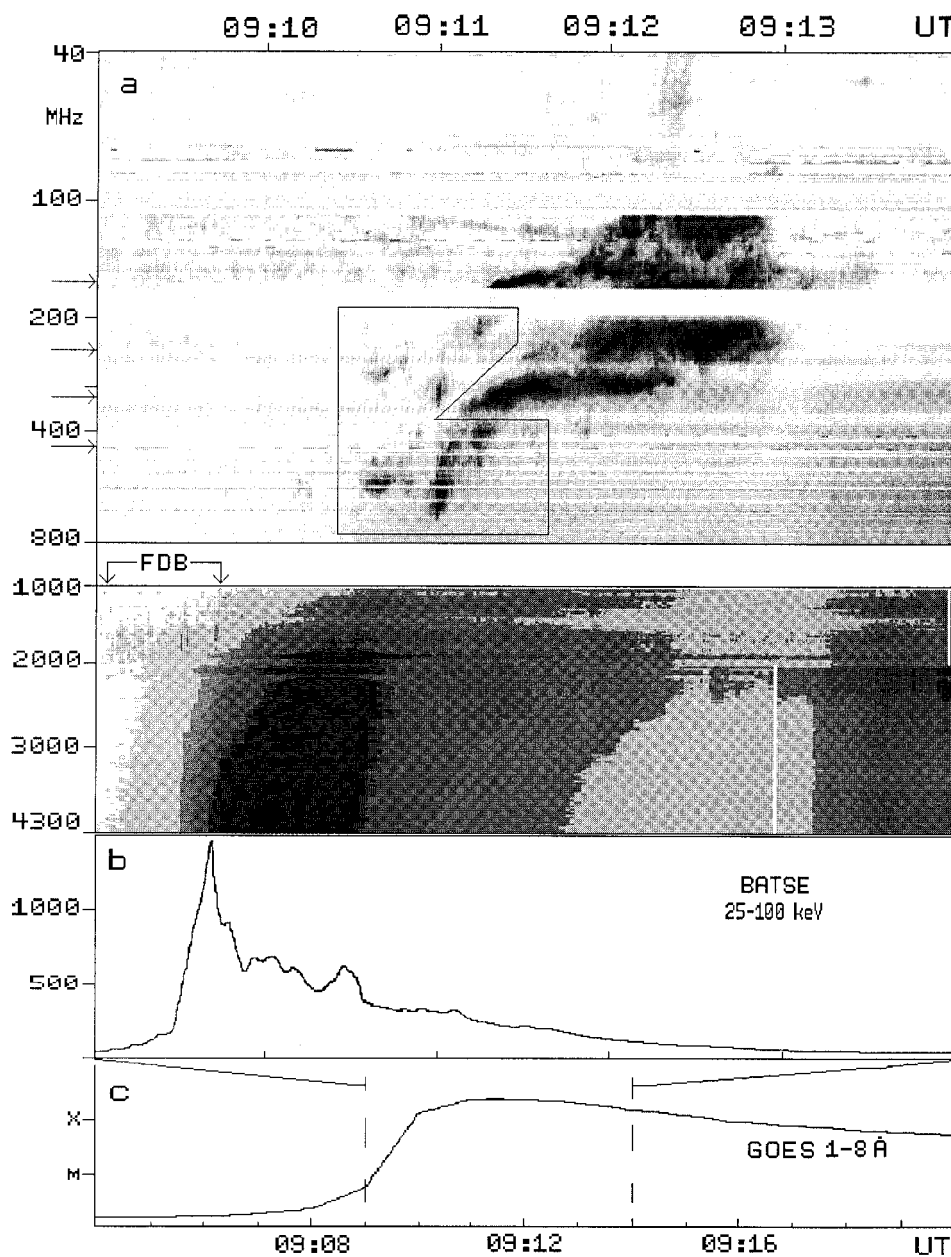


Figure 3. (a) The 40–4300 MHz dynamic spectrum (AI Potsdam and AO Ondřejov) after background subtraction. In the box (a) the first type II (fundamental and harmonic lanes) is shown. The white time-parallel stripes are observational gaps. Arrows indicate the used NRH frequencies. FDB – a group of fast-drift bursts. (b) Hard X-ray fluxes (CGRO BATSE 25–100 keV,  $10^3$  counts  $(s \cdot 2000 \text{ cm}^2)^{-1}$ ). (c) Soft X-ray flux (GOES 1–8 Å,  $X = 10^{-1}$  erg  $(\text{cm} \cdot \text{s})^{-1}$ ).

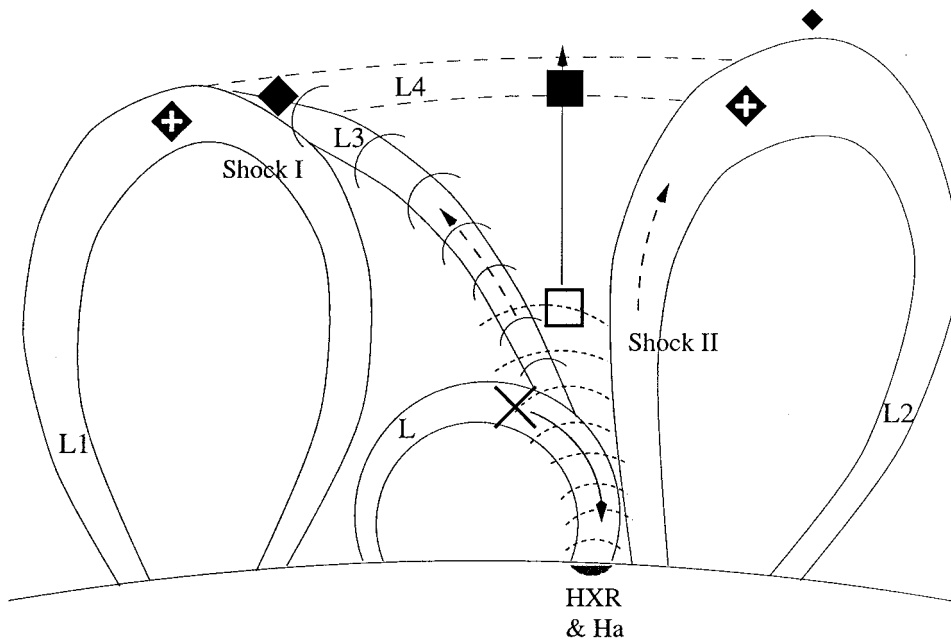


Figure 4. The scenario of the 9 July 1996 flare as seen from upper left corner of Figure 2(a). The designations are used in the same manner as in Figure 2.  $\times$  – the expected primary energy release site. The shock I is expressed by full-line bows, and shock II by dashed-line bows. The full arrow in the  $L$  loop expresses the downward propagating superthermal particles, and the dashed arrows show upward motions of superthermal electrons which are trapped later on at the top of loops L1 and L2 generating the continuum emission.

in the range 1.0–2.0 GHz. At 09:10:30–09:11:30 UT the harmonic mode lanes of the first type II burst occur at 200–750 MHz. Then, at 09:11:07–09:13:10 a second type II burst appears between 80–380 MHz. The first type II burst shows clearer fine structures than the second one. After the decay of the type II bursts (at 09:13:10 UT) a short decrease of the underlying continuum occurred followed by a long-duration repeated recrudescence.

The radio source centroid positions of both type II bursts and of the continuum were determined from the NRH data (courtesy K.-L. Klein). The type II sources are situated above different loop systems. This is confirmed by superposing the radio map onto a *Yohkoh*-SXT image (Figure 2). Both type II sources appear in the different modes\* at various sites. Both the different modes of each burst appear in the same projected distance from the  $H\alpha$  flare site. But the first type II burst is excited further away from the flare site than the second one. Figure 4 redraws schematically the information of Figure 2.

In the harmonic mode, the first type II source is localized near the tops of two loops designated as L3 and L1 (see Figure 4). In the fundamental mode, this source

\*Fundamental and harmonics of the plasma frequency.

is situated in the top of the loop L2. The second type II source appears near to the tops of low-lying loops (L in Figure 4) in the harmonic mode. In the fundamental mode, it scatters around the loop system L1. This is not shown in Figures 2 and 4. The nonalignment of fundamental and harmonic sources can be due to an inherent double source structure of type II bursts (see Aurass, Klein, and Mann, 1994). It can also result from stronger refraction of the fundamental mode.

For an improved discrimination of the different type II bursts we derived the speeds of the exciting disturbance. To do this we used the following methods:

(1) from the frequency drift rate of the burst in the spectrum and a density model of the corona\*, method No. 1 (M1). This method yields the speed component along the local coronal density gradient.

(2) From the heliographic source positions at two frequencies 327 and 236 MHz (M2). This method yields the speed projection on the disc.

(3) From the heliographic source positions and the H $\alpha$  flare site coordinates, using the maximum of the hard X-ray emission as the ignition time of the disturbance (M3).

We obtained the following results:

– The first type II burst source\*\* tended to move westward. A speed cannot be determined because of its short lifetime. The source occurred at about 110 000 km projected distance from the H $\alpha$  flare position.

– The second type II burst source (filled white and black squares at 327 and 236 MHz) occurred only 70 000 km away from the H $\alpha$  flare and reveals an outward motion of the exciter as indicated by the arrow in Figures 2(d) and 4.

– For the first burst two values of the exciter speed are obtained: 3500 km s<sup>-1</sup> (M1) and 2200 km s<sup>-1</sup> (M3). For the second type II burst all three methods are used, we give the results in sequence M1–M3: 1400 km s<sup>-1</sup>, 1200 km s<sup>-1</sup>, 800 km s<sup>-1</sup>. This means the first burst points to a shock being about two times faster than the second one.

– The sources of the continuum emission at 432 and 410 MHz (not shown on Figure 2) during the type II bursts were situated at about the same position as the first type II burst. After the type II disappearance a new double source of moving broadband continuum emission becomes visible. It occurs at the tops of the L1 and L2 (L3) systems and moves in westward and southward directions (black diamonds with white crosses in Figure 4). Pick *et al.* (1997) identified the continuum source sites with the legs of the ongoing huge CME.

Due to the lack of coronagraph images at the time of the flare it is impossible to draw conclusions about relations between the CME, flare and type II bursts. The first coronagraph images were obtained about 3 hours after the flare. At this time, the CME is already at a height of 5 solar radii and has an estimated speed of 450 km s<sup>-1</sup> (Dryer *et al.*, 1998). Both type II bursts reveal much higher exciter speeds.

\*We used the fourfold Newkirk model.

\*\*Big and little black diamonds for harmonic and fundamental emission, respectively.

## 2.4. SUMMARY OF OBSERVATIONS

The presented observations are sketched in Figure 4. In the following we refer to notations in this scheme.

(1) The flare occurs in an AR with a magnetic  $\delta$ -configuration. Newly emerging loops (L) coexist with preexisting larger loop systems L1–L3. We argue that the primary energy release occurs in low-lying loops (L) near to the initial H $\alpha$  kernel but in close touch with large-scale loops.

(2) The impulsive phase of the flare is characterized by microwave and decimeter emission, and a simultaneously appearing group of decimeter fast-drift bursts. The microwave and decimeter bursts start with a negative frequency drift. The fast-drift bursts are associated with the maximum of the HXR emission.

(3) Two type II bursts are spectrally and spatially distinguished. They have different drivers (the first moving twice as fast as the second one) and appear at different positions. Associated radio sources appear at the top of loop systems L1, L2, and L.

(4) At some time intervals, both type II burst sources are simultaneously observed at 327 and 432 MHz in the harmonic mode. The corresponding electron densities are  $N_e = 3.32 \times 10^9$  and  $N_e = 5.76 \times 10^8 \text{ cm}^{-3}$ . The sources are situated about 110 000 km and 70 000 km away from the initial flare site. The type II burst source next to the H $\alpha$  flare (the second type II burst) occurs at lower densities than the distant decimetric type II burst.

## 3. Interpretation

### 3.1. TWO TYPE II BURSTS

Two different shock waves were observed in a complex magnetoplasma geometry as derived from soft X-ray images. The possibility of two different shocks excited by one disturbance follows from numerical simulations by Karlický and Odstrčil (1994, 1998). These authors have shown that shock waves can be generated by the thermal pressure pulse, by the magnetic pressure pulse, or by both disturbances from the energy release site. Although we cannot definitely exclude other shock sources we apply this as a working hypothesis for discussing shock excitation in the present case.

As revealed by the radio spectral data and sketched in Figure 4, the flare energy release starts in low and closed magnetic loops near the H $\alpha$  kernel. This energy release generates MHD disturbances and energetic particles. We expect that the fastest magnetic disturbance\* is guided along neighboring loop structures L2 and L3. The speed of this disturbance is estimated to be 3500–2200 km s $^{-1}$ . The guiding is caused by inhomogeneities in plasma parameters between the inside

\*Triggered by a sudden change of the magnetic field at the primary energy release site.

and outside loops. The quasiparallel moving disturbance manifests as the first type II burst which appears near the top of loops L2 and L3 (see Figure 4). Classen and Mann (1997) have shown that quasiparallel shocks can accelerate electrons thus providing one necessary agent for radio emission. According to Karlický and Odstrčil's (1994) simulations the first shock is of the blast wave type. The relatively short duration of this type II burst is in favour of this fact.

After particle acceleration, the energetic particles propagate downwards and generate the hard X-ray emission. Fast-drift bursts observed at the very beginning of the flare near 1.5 GHz (Figure 2(a)) confirm the presence of particle beams at high densities. The primary energy release site has no access to open coronal field lines. No metric type III bursts were observed during the impulsive phase.

With some time delay\*, a rising evaporation front is generated at the flare loop footpoints. It propagates upwards as a hydrodynamic disturbance and later on as a hydrodynamic shock. Thereby, superthermal particles generated during the impulsive phase can diffuse toward neighboring larger loops where they become trapped. This is confirmed by the continuum emission from the tops of L1 and L2 and is in accordance with Robinson (1985). At a site with minimum background Alfvén speed (between loops L2 and L3 in Figure 4) the disturbance is transformed into a super-Alfvénic MHD disturbance. The second type II burst appears. As predicted, it starts in relatively low heights between loops identified in soft X-ray images (Figure 4). The second shock is slower (800–1400 km s<sup>-1</sup>) than the first one. We assume it is driven by the evaporation front acting like a piston. It exists for a longer time than the first type II burst, thereby forming the main type II burst pattern displayed by the radio spectrum.

During the flare, the loop L3 is moving upwards and the central part of the magnetic field above the AR is restructured (see the dashed loop L4 in Figure 4). This change in the magnetic field structure can be taken as favoring the model of a piston-driven type II burst.

### 3.2. THE DRIFTING CENTIMETER–DECIMETER BURST

The microwave-decimeter burst starting before the discussed type II emission demands some attention by its 'drifting' onset behavior which is not typical in this spectral range. This emission can be due to two different mechanisms:

- the gyrosynchrotron mechanism connected with precipitating particles of varying energy spectrum or with changing precipitation sites (Robinson, 1985; Bruggmann *et al.*, 1990; Karlický, 1991), and
- the plasma emission mechanism connected with MHD and hydrodynamic shocks (Karlický and Odstrčil, 1994; Karlický, 1998).

Karlický (1998) argues that the low frequency part of the drifting burst is the radio manifestation of the evaporation shock. Due to the particle bombardment of dense layers, the hydrodynamic evaporation shock is generated. Particle beams

\*Due to heating processes.

excite, in the shock vicinity, Langmuir waves which are then transformed into electromagnetic ones. But dense layers are optically thick. So, the electromagnetic radiation should be absorbed in these layers. On the other hand, within the evaporation front the optical thickness of the 1–4 GHz plasma radio emission will be strongly reduced\*. Therefore the optical thickness reduction rises like a visibility window with the evaporation front. A rising window for plasma radio emission would result in the drifting microwave–decimeter burst.

Karlíček's (1998) interpretation nicely fits with the type II burst analysis presented above. Nevertheless, this is only an indirect hint and we are not yet able to firmly distinguish between the gyrosynchrotron and the plasma mechanisms.

#### 4. Conclusions

A sequence of two type II radio bursts during one flare event has been analyzed in this paper. The first shock was initiated by a magnetic disturbance generated during the impulsive phase. The disturbance was found to be guided within loop structures identified by *Yohkoh* soft X-ray images and Nançay radio imaging data. It evolved into a quasi-parallel shock which is observed as a first (higher-frequency) type II burst at the top of an extended loop system.

The second type II burst was observed with some time delay and nearer to the H $\alpha$  flare site. The source was situated between extended loop systems. The second type II burst was probably driven from the evaporation shock which is initiated as a response of dense atmospheric layers to the particle bombardment.

The present study tried to elucidate the processes which generated several shocks during one flare event. A next step should be the comparison of the observed facts with detailed numerical MHD simulations.

#### Acknowledgements

The authors thank Dr K.-L. Klein (Paris-Meudon Observatory) for the radio imaging data and for critical and stimulating discussions. Further, the authors are thankful for the access to the *Yohkoh* data at Mullard Space Center and BATSE/CGRO and GOES data at the Solar Data Analysis Center at NASA/GSFC. The authors also want to express many thanks to Dr Barbara Thompson and the SOHO/MDI team for magnetic data, Dr Alan Kiplinger for the H $\alpha$  data, and the Mount Wilson Observatory for sunspot drawings shown on the webpage. The comments of an unknown referee essentially improved the presentation of the paper.

We acknowledge the support from the grants A3003707 of the Academy of Sciences of Czech Republic and Au106/6-2 of the Deutsche Forschungsgemeinschaft.

\*Due to the sharp parameter jump and the temperature increase.

M. Karlický thanks the radio group of Astrophysikalisches Institut Potsdam for its hospitality.

### References

- Aurass, H.: 1997, in G. Trottet (ed.), *Lecture Notes in Physics* **483**, 135.
- Aurass, H., Klein, K.-L., and Mann, G.: 1994, ESA- SP-373, p. 95.
- Aurass, H., Mann, G., Dryer, M., Andrews, M. D., Michels, D. J. Paswaters, S. E., and Tappin, S. J.: 1997, in Proc. Fifth SOHO Workshop, ESA ISP-404, p. 183.
- Bruggmann, G., Benz, A., Magun, A., and Stehling, W.: 1990, *Astron. Astrophys.* **240**, 506.
- Classen, H.-T. and Mann, G.: 1997, *Astron. Astrophys.* **322**, 696.
- Dryer, M., Andrews, M. D., Aurass, H., DeForest, C., Karlický, M., Kiplinger, A., Klassen, A., Meisner, R., Ipavich, F. M., Galvin, A. B., Paswaters, S. E., Smith, Z., Tappin, S. J., Thompson, B. J., Watari, S.-I., Michels, D. J., Bruckner, G. E., Howard, R. A., Koomen, M. J., Lamy, P., Mann, G., Arzner, K., and Schwenn, R.: 1998, *Solar Phys.* **181**, 159.
- Forbes, T. G. and Priest, E. R.: 1983, *Solar Phys.* **84**, 169.
- Gopalswamy, N. and Kundu, M. R.: 1992, in G. P. Zank and T. K. Gaiser (eds.), *Particle Acceleration in Cosmic Plasmas*, American Institute of Physics, New York, p. 257.
- Gopalswamy, N., Kaiser, M. R., Lepping, R. P., and 6 co-authors: 1998, *J. Geophys. Res.* **103**, 307.
- Hudson, H. S., LaBonte, B. J., Sterling, A. C., Watanabe, T.: 1998, in T. Watanabe, T. Kosugi, and A. C. Sterling (eds.), *Observational Plasma Astrophysics: Five Years of Yohkoh and Beyond*, Astrophys. and Space Science Library, Vol. 229, Kluwer Academic Publishers, Dordrecht, p. 237.
- Jiříčka, K., Karlický, M., Kepka, O., and Tlamicha, A.: 1993, *Solar Phys.* **147**, 203.
- Karlický, M.: 1988, *Bull. Astron. Inst. Czech.* **39**, 13.
- Karlický, M.: 1991, *Bull. Astron. Inst. Czech.* **42**, 260.
- Karlický, M.: 1998, *Astron. Astrophys.* **338**, 1084.
- Karlický, M. and Odstrčil, D.: 1994, *Solar Phys.* **155**, 171.
- Karlický, M., Odstrčil, D., Klassen, A., and Aurass, H.: 1998, *1998 Fall Meeting*, AGU, Vol. 79, No. 45, F712.
- Klassen, A., Aurass, H., Klein, K.-L., Hofmann, A., and Mann, G.: 1999, *Astron. Astrophys.* **343**, 287.
- Klein, K.-L., Klassen, A., and Aurass, H., LASCO Consortium: 1997, *Proc. Fifth SOHO Workshop*, ESA SP-404, p. 461.
- Kosovichev, A. G. and Zharkova, V. V.: 1998, *Nature* **393**, 317.
- Kosugi, T.: 1993, in J. Linsky and S. Serio (eds.), *Physics of Solar and Stellar Coronae*, Kluwer Academic Publishers, Dordrecht, p. 131.
- Mann, G.: 1995, in A. O. Benz and A. Krüger (eds.), *Lecture Notes in Physics* **444**, 183.
- Mann, G. and Classen, H.-T.: 1995, *Astron. Astrophys.* **304**, 576.
- Mann, G., Classen, H.-T., and Aurass, H.: 1995, *Astron. Astrophys.* **295**, 775.
- Mann, G., Aurass, H., Voigt, W., and Paschke, J.: 1992, ESA SP-348, p. 129.
- Mann, G., Aurass, H., Classen, H.-T., Klassen, A., Dröge, W., and Kunow, H.: 1997, *Proc. Fifth SOHO Workshop*, ESA SP-404, p. 543.
- Nelson, G. J. and Melrose, D. R.: 1985, in D. J. McLean and N. R. Labrum (eds), *Solar Radiophysics*, Cambridge University Press, Cambridge, p. 333.
- Nelson, G. J. and Robinson, R. D.: 1975, *Proc. Astron. Soc. Australia* **2**, 370.
- Pick, M., Maia, D., Howard, R., Kerdraon, A., Brueckner, G. E., Lamy, P., Schwenn, R., Aurass, H.: 1997, *Proc. Fifth SOHO Workshop*, ESA SP-404, p. 601.
- Priest, E. R.: 1996, in R. D. Bently and J. T. Mariska (eds.), 'Magnetic Reconnection in the Solar Atmosphere', *Publ. Astron. Soc. Japan* **111**, 331.

- Robinson, R. D.: 1985, in D. J. McLean and N. R. Labrum (eds.), *Solar Radiophysics*, Cambridge University Press, Cambridge, p. 385.
- Robinson, R. D. and Stewart, R. T.: 1985, *Solar Phys.* **97**, 145.
- Scherrer, P. H., Bogart, R. S., Bush, R. I., Hoeksema, J. T., Kosovichev, A. G., Schou, J., Rosenberg, W., Springer, L., Tarbell, T. D., Title, A., Wolfson, C. J., and Zayer, I.: 1995, *Solar Phys.* **162**, 129.
- Sheeley, N. R., Stewart, R. T., Robinson, R. D., Howard, R. A., Kooman, M. J., and Michels, D. J.: 1984, *Astrophys. J.* **279**, 839.
- Somov, B. V.: 1992, *Physical Processes in Solar Flares*, Kluwer Academic Publishers, Dordrecht, p. 49.
- Stewart, R. T.: 1977, *Proc. Astron. Soc. Australia* **3**, 157.
- Tandberg-Hanssen, E., and Emslie, A. G.: 1988, *The Physics of Solar Flares*, Cambridge University Press, Cambridge, p. 177.
- The Radioheliograph Group: 1993, *Adv. Space Res.* **13**(9), 441.
- Tsuneta, S. and Naito, T.: 1998, *Astrophys. J.* **495**, L67.
- Tsuneta, S., Acton, L., Bruner, M., Lemen, J., Brown, W., Carvalho, R., Catura, R., Freeland, S., Jurcevic, B., Morrison, M., Ogawara, Y., Hirayama, T., and Owens, J.: 1991, *Solar Phys.* **136**, 37.
- Ugai, M.: 1982, *Phys. Fluids* **25**, 1027.
- Vršnak, B., Ruždjak, V., Zlobec, P., and Aurass, H.: 1995, *Solar Phys.* **158**, 331.
- Wagner, W. J. and MacQueen R. M.: 1983, *Astron. Astrophys.* **120**, 136.